

Proton Assisted Reduction of CO₂ by Cobalt Aminopyridine Macrocycles

Alon Chapovetsky,[‡] Thomas H. Do,[‡] Ralf Haiges,[‡]
Michael K. Takase,[†] Smaranda C. Marinescu^{*‡}

[‡]Department of Chemistry, University of Southern California, Los Angeles, California 90089, United States

[†]Beckman Institute, California Institute of Technology, Pasadena, California 91125, United States

* E-mail: smarines@usc.edu

General

All manipulations of air and moisture sensitive materials were conducted under a nitrogen atmosphere in a Vacuum Atmospheres drybox or on a dual manifold Schlenk line. The glassware was oven-dried prior to use. All solvents were degassed with nitrogen and passed through activated alumina columns and stored over 4Å Linde-type molecular sieves. Deuterated solvents were dried over 4Å Linde-type molecular sieves prior to use. Proton NMR spectra were acquired at room temperature using Varian (Mercury 400 2-Channel, VNMRS-500 2-Channel, VNMRS-600 3-Channel, and 400-MR 2-Channel) spectrometers and referenced to the residual ¹H resonances of the deuterated solvent (¹H: CDCl₃, δ 7.26; C₆D₆, δ 7.16; CD₂Cl₂, δ 5.32; CD₃CN, δ 2.94) and are reported as parts per million relative to tetramethylsilane. Elemental analyses were performed using Thermo Scientific™ FLASH 2000 CHNS/O Analyzers. All the chemical reagents were purchased from commercial vendors and used without further purification. The ligands (**L**¹⁻³) were prepared according to the reported literature procedures.¹

Electrochemistry experiments were carried out using a Pine potentiostat. The experiments were performed in a single compartment electrochemical cell under nitrogen or CO₂ atmosphere using a 3 mm diameter glassy carbon electrode as the working electrode, a platinum wire as auxiliary electrode and a silver wire as the reference electrode. All experiments in this paper were referenced relative to ferrocene (Fc) with the Fe^{3+/2+} couple at 0.0 V using Fc or decamethylferrocene (Fc*) as an internal standard. All electrochemical experiments were performed with 0.1 M tetrabutylammonium hexafluorophosphate as supporting electrolyte. Cobalt complex concentrations were generally at 0.5 mM and experiments with CO₂ were performed at gas saturation in dimethylformamide (DMF).

Controlled-potential electrolysis measurements were conducted in a two-chambered H cell. The first chamber held the working and reference electrodes in 50 mL of 0.1 M tetrabutylammonium hexafluorophosphate and 0.5 M methanol in DMF. The second chamber held the auxiliary electrode in 25 mL of 0.1 M tetrabutylammonium hexafluorophosphate in DMF. The two chambers were separated by a fine porosity glass frit. The reference electrode was placed in a separate compartment and connected by a Vycor tip. Glassy carbon plate electrodes (6 cm × 1 cm × 0.3 cm; Tokai Carbon USA) were used as the working and auxiliary electrodes. The experiments were referenced relative to ferrocene (Fc) with the Fe^{3+/2+} couple at 0.0 V using Fc

or decamethylferrocene (Fc*) as an internal standard. Gas analysis for controlled potential electrolysis experiments were performed using 10 mL sample aliquots taken from the headspace of the electrochemical cell and injected on a Shimadzu BID-2010 plus series gas chromatograph with a 2m × 1mm ID micropacked column. Faradaic efficiencies were determined by dividing the measured CO produced by the amount of CO expected based on the charge passed during the bulk electrolysis experiment. For each species the controlled-potential electrolysis measurements were performed at least twice, leading to similar behavior. The reported Faradaic efficiencies and mmol of CO produced are average values.

[Co(L¹)(acetone)₂][BF₄]₂ (1). [Co(H₂O)₆][BF₄]₂ (14.3 mg, 0.0419 mmol) in acetone (1 mL) was added to a solution of L¹ (15.6 mg, 0.0423 mmol) in acetone (2 mL) giving rise to a brown solution. The mixture was allowed to stir for 5 minutes. The solution was filtered through a microfiber filter. Slow diffusion with diethyl ether produced orange crystals in quantitative yields. ¹H NMR (400 Hz, MeCN-*d*₃) δ 35.88 (s, 8H, *m*-NC₅H₃), 14.07 (s, 4H, *p*-NC₅H₃), 3.01 (s, 4H, NH). Anal. calcd for [Co(L¹)]₂·3MeCOMe·0.5H₂O (C₂₉H₃₆B₂CoF₈N₈O₄): C, 43.78; H, 4.57; N, 14.13. Found: C, 43.91; H, 4.11; N, 14.53.

[Co(L²)(MeCN)][BF₄]₂ (2). [Co(H₂O)₆][BF₄]₂ (14.3 mg, 0.0419 mmol) in acetone (1 mL) was added to a solution of L² (16.6 mg, 0.0391 mmol) in dichloromethane (2 mL) giving rise to a brown solution. The mixture was allowed to stir for 5 minutes. The volatiles were removed under vacuum, and the amber solid was dissolved in acetonitrile and the solution was filtered through a microfiber filter. Slow diffusion with diethyl ether produced orange crystals in quantitative yields. ¹H NMR (400 Hz, MeCN-*d*₃) δ 10.66 (s, 4H, *p*-NC₅H₃), 4.94 (s, 8H, *m*-NC₅H₃), 2.67 (s, 12H, NMe). Anal. calcd for [Co(L²)]₂·MeCOMe·MeCN (C₃₁H₃₆B₂CoF₈N₁₀O): C, 46.81; H, 4.28; N, 17.16. Found: C, 46.70; H, 4.55; N, 17.57.

[Co(L³)(H₂O)][BF₄]₂ (3). [Co(H₂O)₆][BF₄]₂ (11 mg, 0.032 mmol) in acetone (1 mL) was added to a solution of L³ (16.7 mg, 0.031 mmol) in dichloromethane (2 mL) giving rise to a brown solution. The mixture was allowed to stir for 30 minutes. The solvent was removed under vacuum and the solids were dissolved in dichloromethane (2 mL). Slow diffusion with diethyl ether produced yellow crystals in quantitative yields. ¹H NMR (400 Hz, MeCN-*d*₃) δ 9.49 (s, 4H, *p*-NC₅H₃), 4.61-5.32 (m, 20H), 3.69 (s, 8H). Anal. calcd for [Co(L³)]₂·H₂O (C₃₂H₃₄B₂CoF₈N₈O): C, 49.33; H, 4.40; N, 14.38. Found: C, 49.23; H, 4.51; N, 14.38.

[Zn(L¹)]₂[BF₄]₂. A solution of Zn(BF₄)₂ hydrate (11 mg, 0.032 mmol) in acetone (1 mL) was added to a solution of L¹ (16.7 mg, 0.031 mmol) in acetone (2 mL) giving rise to an amber solution. The mixture was allowed to stir for 5 minutes. Slow diffusion with diethyl ether produced amber crystals in quantitative yields. ¹H NMR (500 Hz, MeCN-*d*₃) δ 8.31 (s, 4H, NH), 7.85 (t, 4H, *p*-NC₅H₃), 6.94 (s, 8H, *m*-NC₅H₃). Anal. calcd for [Zn(L¹)]₂·MeCOMe·(H₂O)₂ (C₂₃H₂₆B₂ZnF₈N₈O₃): C, 39.38; H, 3.74; N, 15.97. Found: C, 39.59; H, 3.25; N, 15.45

[Co(L¹)(Pyridine)₂][BF₄]₂ (4). A solution of compound 1 (14 mg, 0.023 mmol) dissolved in pyridine (2 mL) and cooled to -35 °C. The solution was added to cold KC₈ (5.8 mg, 0.043 mmol). The vial was capped and agitated for 30 seconds, giving rise to a green solution. The solution was filtered to remove graphite and potassium tetrafluoroborate. Slow diffusion with diethyl ether produced amber crystals in quantitative yields. ¹H NMR (500 Hz, pyridine-*d*₅) δ

33.39 (s, 8H, *m*-NC₅H₃), 11.2 (s, 4H, *p*-NC₅H₃), 4.84 (s, 4H, NH). Anal. calcd for [Co(L¹)] [BF₄]⁻·(C₅H₅N)₃ (C₃₅H₃₁BCoF₄N₁₁): C, 55.94; H, 4.16; N, 20.5. Found: C, 55.95; H, 4.00; N, 18.61.

Complexes **1–3** were characterized by ¹H NMR spectroscopy in MeCN-*d*₃. Two broad paramagnetic peaks at δ 35.8 and 14.1 ppm are observed for complex **1** in the 2:1 ratio, which correspond to the *meta* and *para* protons of the pyridine moiety, respectively. A single peak at 3.1 ppm was assigned to the amine protons. Complex **2** displays three broad peaks at δ 10.66, 4.94, and 2.67 ppm in the 1:2:3 ratio, corresponding to the *para* and *meta* protons of the pyridine moiety, and the *NMe* protons, respectively. Similarly, complex **3** displays broad peaks at δ 9.49, 4.61–5.32, and 3.69 ppm, corresponding to the protons of the pyridine and allyl groups.

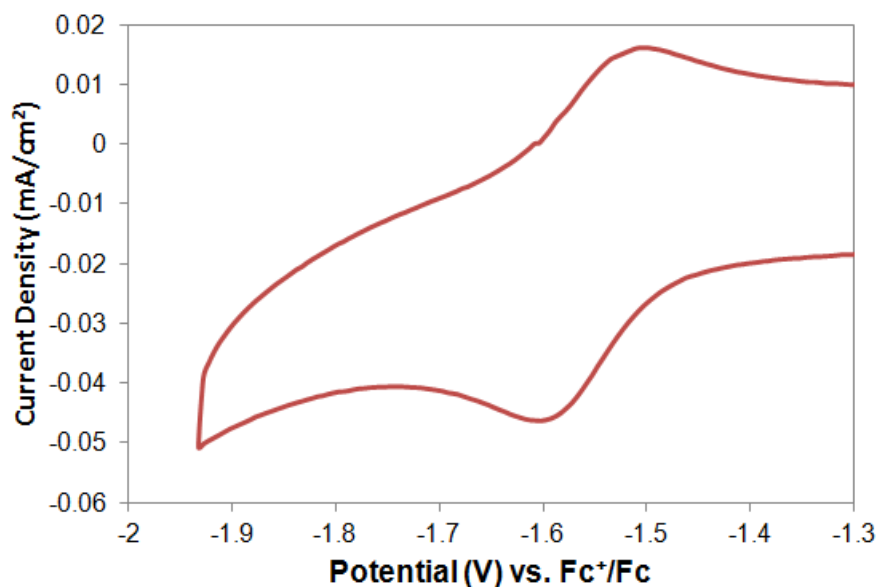


Figure S1. Cyclic voltammograms of 0.5 mM [Co(L¹)(H₂O)] [BF₄]₂ (**1**) in a DMF solution containing 0.1 M [*n*Bu₄N] [PF₆]⁻ under an atmosphere of N₂ displaying the Co^{II/I} redox couple. Scan rate is 100 mV/s.

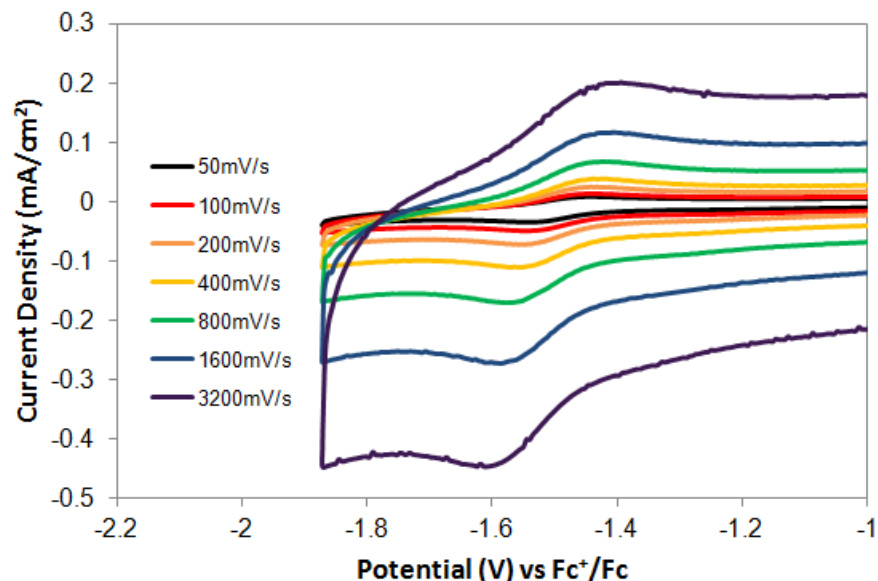


Figure S2. Cyclic voltammogram scan rate dependence of 0.5 mM [Co(L¹)(H₂O)][BF₄]₂ (**1**) in a DMF solution containing 0.1 M [nBu₄N][PF₆] under an atmosphere of N₂ displaying the Co^{II/I} redox couple. Scan rates vary from 50 to 3200 mV/s.

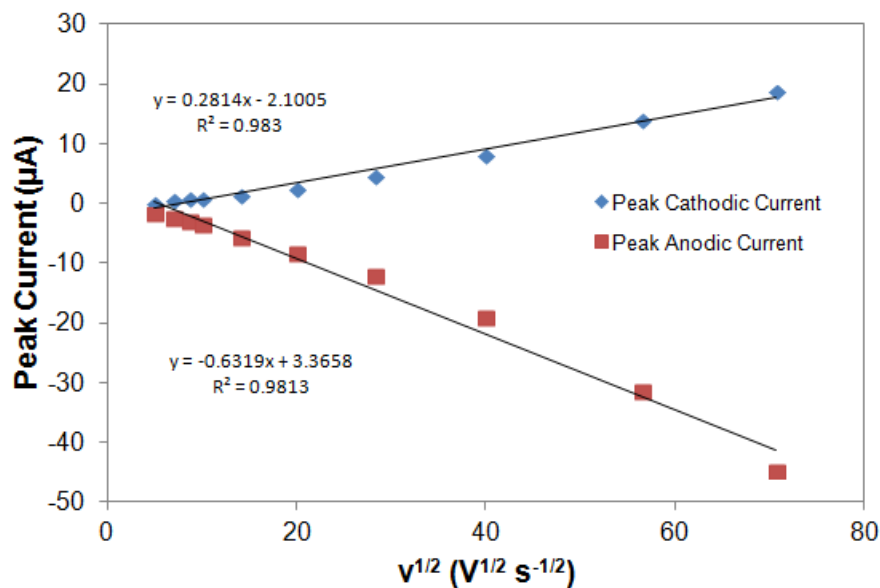


Figure S3. Plot showing that the peak current, both cathodic and anodic, in the cyclic voltammograms (CVs) of 0.5 mM [Co(L¹)(H₂O)][BF₄]₂ (**1**) in a DMF solution containing 0.1 M [nBu₄N][PF₆] under an atmosphere of N₂. The cathodic and anodic peak currents increase linearly with the square root of the scan rate. This behavior is indicative of a freely-diffusing species, where the electrode reaction is controlled by mass transport.

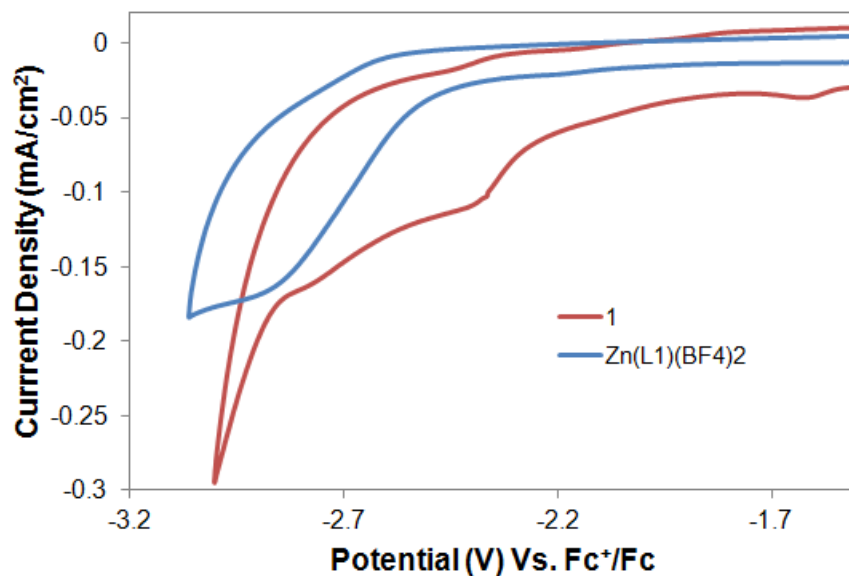


Figure S4. Cyclic voltammogram of 0.5 mM of $[\text{Co}(\text{L}^1)][\text{BF}_4]_2$ (**1**) (red) and $[\text{Zn}(\text{L}^1)][\text{BF}_4]_2$ (blue) in a DMF solution containing 0.1 M $[\text{nBu}_4\text{N}][\text{PF}_6]$ under an atmosphere of N_2 . Scan rate is 100 mV/s.

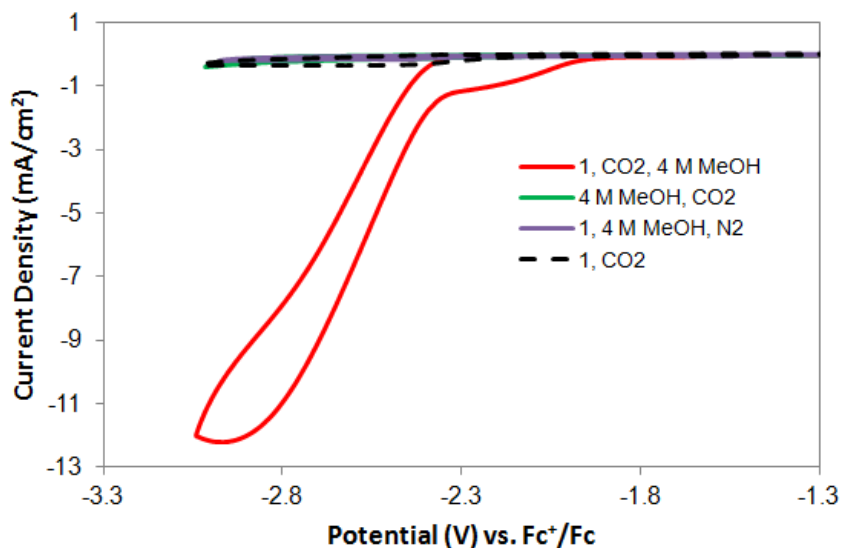


Figure S5. Cyclic voltammograms of 0.5 mM $[\text{Co}(\text{L}^1)(\text{H}_2\text{O})][\text{BF}_4]_2$ (**1**) in a DMF solution containing 0.1 M $[\text{nBu}_4\text{N}][\text{PF}_6]$ and methanol (4 M) under an atmosphere of CO_2 (red), and N_2 (purple), and control experiments in the absence of protons (black dashed), and catalyst (green). Scan rate is 100 mV/s.

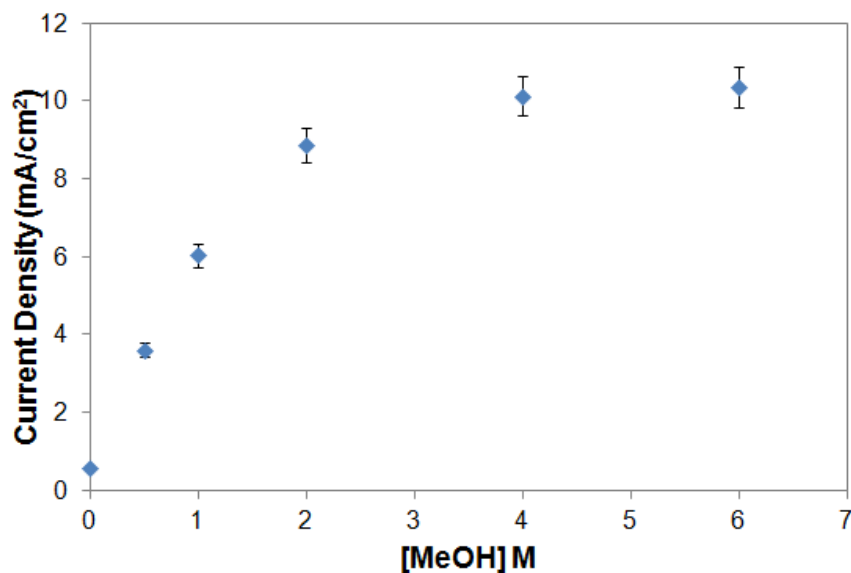


Figure S6. Plot of maximum current density measured at -2.75 V (vs. $\text{Fc}^{+/0}$) vs. $[\text{MeOH}]$ for cyclic voltammograms of 0.5 mM $[\text{Co}(\text{L}^1)(\text{H}_2\text{O})][\text{BF}_4]_2$ (**1**) in a DMF solution containing 0.1 M $[\text{nBu}_4\text{N}][\text{PF}_6]$ under an atmosphere of CO_2 and in the presence of varying concentrations of methanol. The measured current densities are determined as the average of two independent measurements. At high $[\text{MeOH}]$, i_{cat} reaches a limiting value independent of $[\text{MeOH}]$, which is typical of saturation kinetics expected for catalytic reactions.

$[\text{MeOH}]$ (M)	$i_{\text{cat}}/i_{\text{p}}$
0.5	19.0
1	31.8
2	46.7
4	53.4
5	54.0
6	54.6

Table S1. Table of the peak $i_{\text{cat}}/i_{\text{p}}$ values measured at -2.75 V (vs. $\text{Fc}^{+/0}$) for 0.5 mM $[\text{Co}(\text{L}^1)(\text{H}_2\text{O})][\text{BF}_4]_2$ (**1**) in a DMF solution containing 0.1 M $[\text{nBu}_4\text{N}][\text{PF}_6]$ under an atmosphere of CO_2 and with varying amounts of methanol.

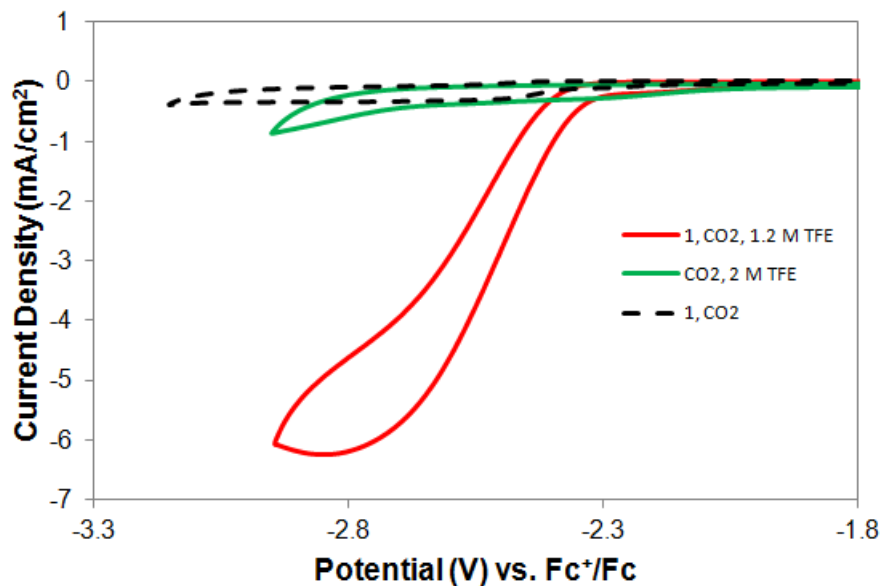


Figure S7. Cyclic voltammograms of 0.5 mM $[\text{Co}(\text{L}^1)(\text{H}_2\text{O})][\text{BF}_4]_2$ (**1**) in a DMF solution containing $[\text{nBu}_4\text{N}][\text{PF}_6]$ (0.1 M), 2,2,2-trifluoroethanol (1.2 M), and CO_2 (1 atm) – red; and in the absence of 2,2,2-trifluoroethanol (black dashed), or catalyst (green). The increase in current under CO_2 and TFE is attributed to catalysis from CO_2 to CO. Scan rate is 100 mV/s.

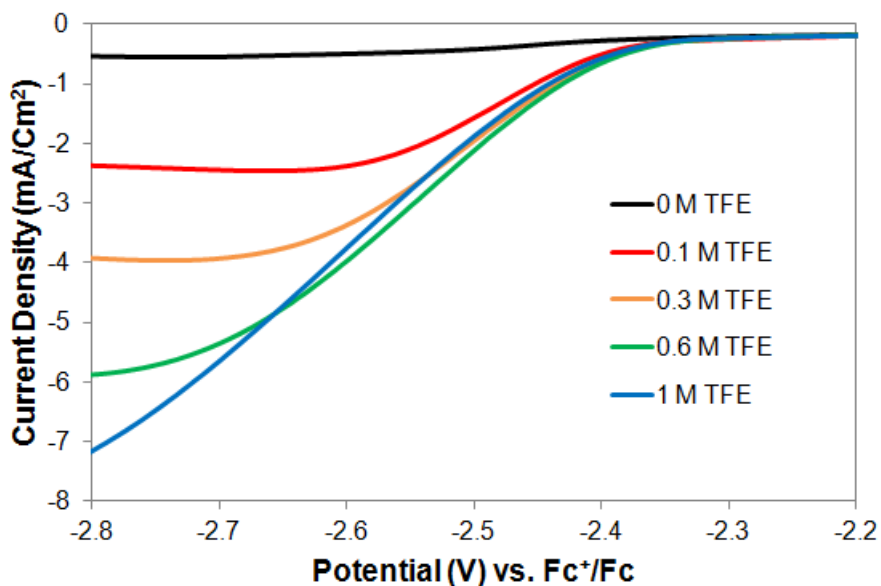


Figure S8. Linear scan voltammograms of **1** (0.5 mM) in a DMF solution containing 0.1 M $[\text{nBu}_4\text{N}][\text{PF}_6]$ under an atmosphere of CO_2 and in the presence of varying concentrations of 2,2,2-trifluoroethanol. Scan rates are 100 mV/s.

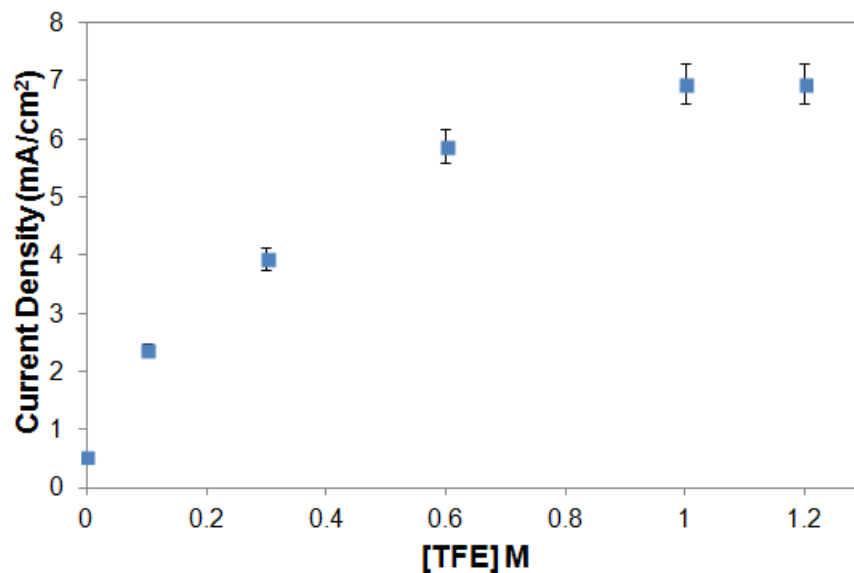


Figure S9. Plot of maximum current density measured at -2.75 V (vs. $\text{Fc}^{+/0}$) vs. [TFE] for cyclic voltammograms of 0.5 mM $[\text{Co}(\text{L}^1)(\text{H}_2\text{O})][\text{BF}_4]_2$ (**1**) in a DMF solution containing 0.1 M $[\text{nBu}_4\text{N}][\text{PF}_6]$ under an atmosphere of CO_2 and varying concentrations of 2,2,2-trifluoroethanol. The measured current densities are determined as the average of two independent measurements. At high [TFE], i_{cat} reaches a limiting value independent of [TFE], which is typical of saturation kinetics expected for catalytic reactions.

[TFE] (M)	$i_{\text{cat}}/i_{\text{p}}$
0.1	8.6
0.3	15.1
0.6	21.2
1	22.7
1.2	24.2

Table S2. Table of the peak $i_{\text{cat}}/i_{\text{p}}$ values measured at -2.75 V (vs. $\text{Fc}^{+/0}$) for 0.5 mM $[\text{Co}(\text{L}^1)(\text{H}_2\text{O})][\text{BF}_4]_2$ (**1**) in a DMF solution containing 0.1 M $[\text{nBu}_4\text{N}][\text{PF}_6]$ under an atmosphere of CO_2 and with varying amounts of 2,2,2-trifluoroethanol.

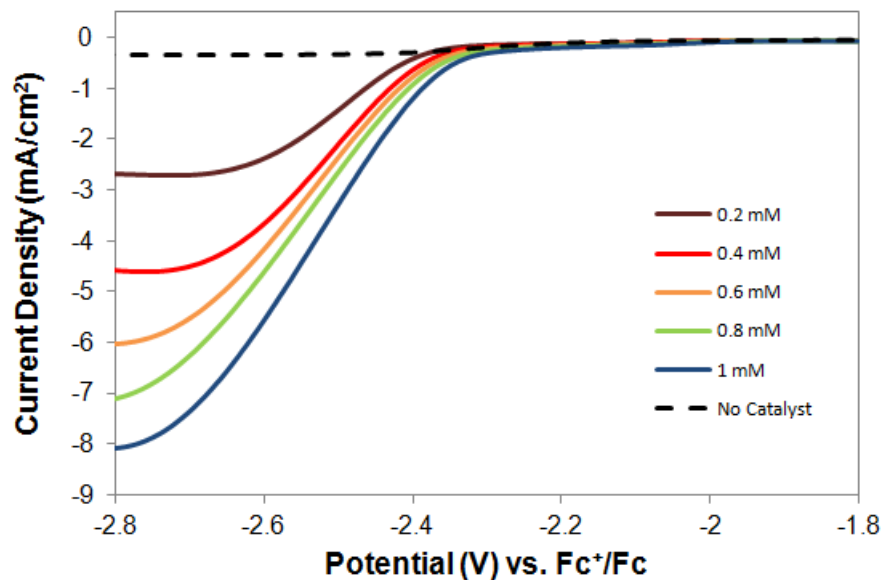


Figure S10. Cyclic voltammograms showing catalytic current for $[\text{Co}(\text{L}^1)(\text{H}_2\text{O})][\text{BF}_4]_2$ (**1**) in a DMF solution containing 0.1 M $[\text{nBu}_4\text{N}][\text{PF}_6]$ under an atmosphere of CO_2 and in the presence of methanol (2 M). The concentration of **1** is varied from 0.2 to 1 mM. Scan rates are 100 mV/s.

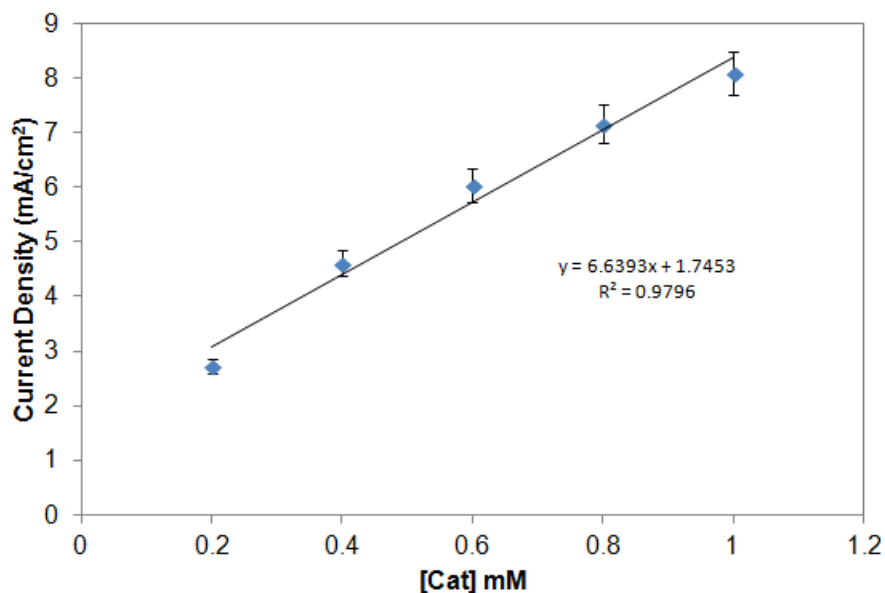


Figure S11. Plot of maximum current density measured at -2.8 V (vs. $\text{Fc}^{+/0}$) vs. $[\text{cat}]$ for cyclic voltammograms of $[\text{Co}(\text{L}^1)(\text{H}_2\text{O})][\text{BF}_4]_2$ (**1**) in a DMF solution containing 0.1 M $[\text{nBu}_4\text{N}][\text{PF}_6]$ under an atmosphere of CO_2 and in the presence of methanol (2 M). The measured current densities are determined as the average of two independent measurements. The concentration of **1** is varied from 0.2 to 1 mM. A linear dependence on the catalyst concentration is observed.

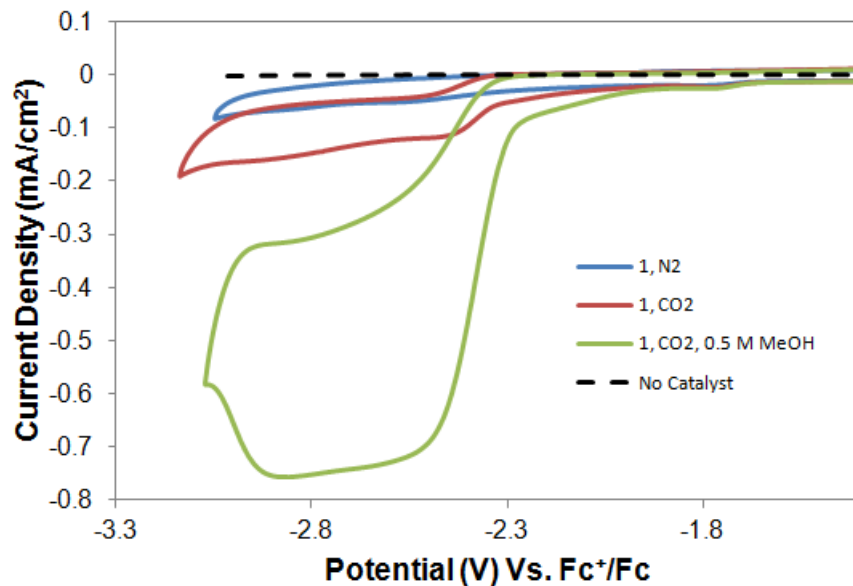


Figure S12. Cyclic voltammogram of 0.2 mM $[\text{Co}(\text{L}^1)(\text{H}_2\text{O})][\text{BF}_4]_2$ (**1**) in a DMSO solution containing 0.1 M $[\text{nBu}_4\text{N}][\text{PF}_6]$ under an atmosphere of N_2 (blue), CO_2 (red), and CO_2 with 0.5 M MeOH (green). Scan rate is 100 mV/s.

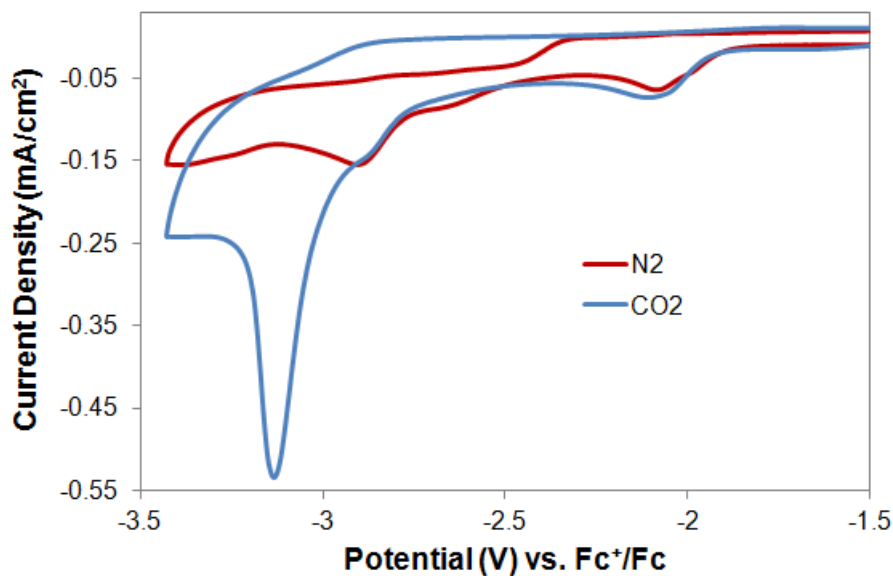


Figure S13. Cyclic voltammogram of 0.5 mM of $[\text{Co}(\text{L}^1)][\text{BF}_4]_2$ (**1**) in a 1:4 mixture of DMF:acetonitrile solutions containing 0.1 M $[\text{nBu}_4\text{N}][\text{PF}_6]$ under an atmosphere of N_2 (red) or CO_2 (blue). Scan rate is 100 mV/s.

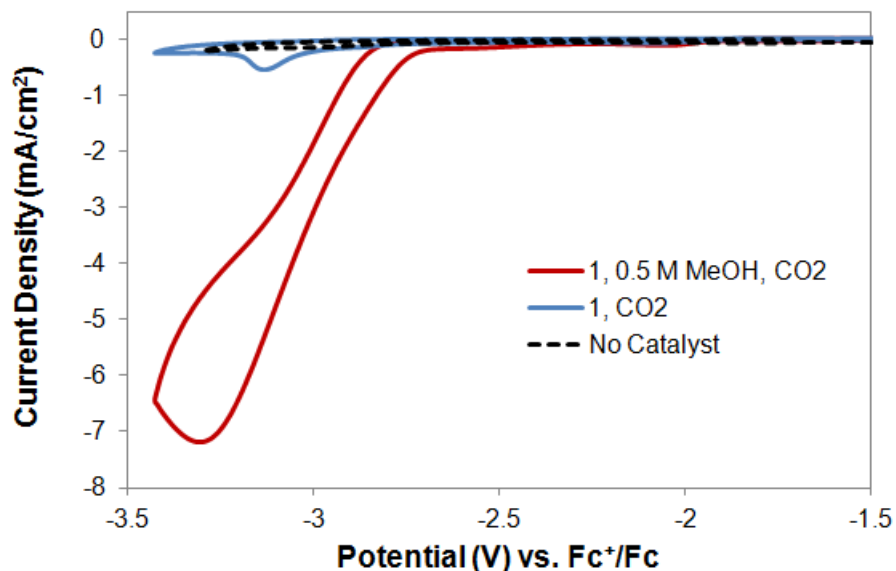


Figure S14. Cyclic voltammogram of 0.5 mM $[\text{Co}(\text{L}^1)][\text{BF}_4]_2$ (**1**) in a 1:4 mixture of DMF:acetonitrile solutions containing 0.1 M $[\text{nBu}_4\text{N}][\text{PF}_6]$ under an atmosphere of CO_2 with 0.5 M MeOH (red), and in the absence of methanol (blue), or catalyst (black dashed). Scan rate is 100 mV/s.

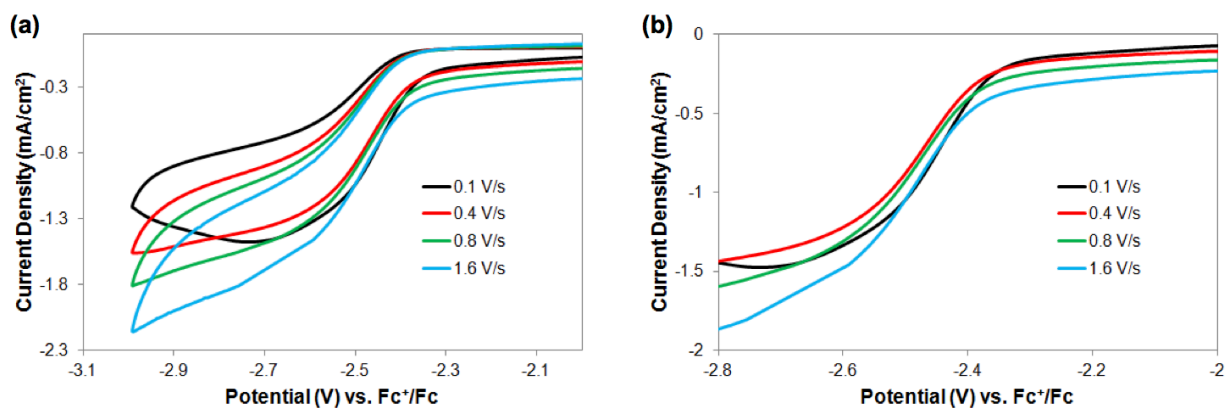


Figure S15. Cyclic voltammogram scan rate dependence studies of 0.1 mM $[\text{Co}(\text{L}^1)(\text{H}_2\text{O})][\text{BF}_4]_2$ (**1**) in a DMF solution containing 0.1 M $[\text{nBu}_4\text{N}][\text{PF}_6]$ under an atmosphere of CO_2 and in the presence of 2,2,2-trifluoroethanol (0.6 M). Under these conditions catalyst **1** displays catalytic waves as idealized, canonical 'S-shaped', that are scan rate independent. Scan rates vary from 100 to 1600 mV/s.

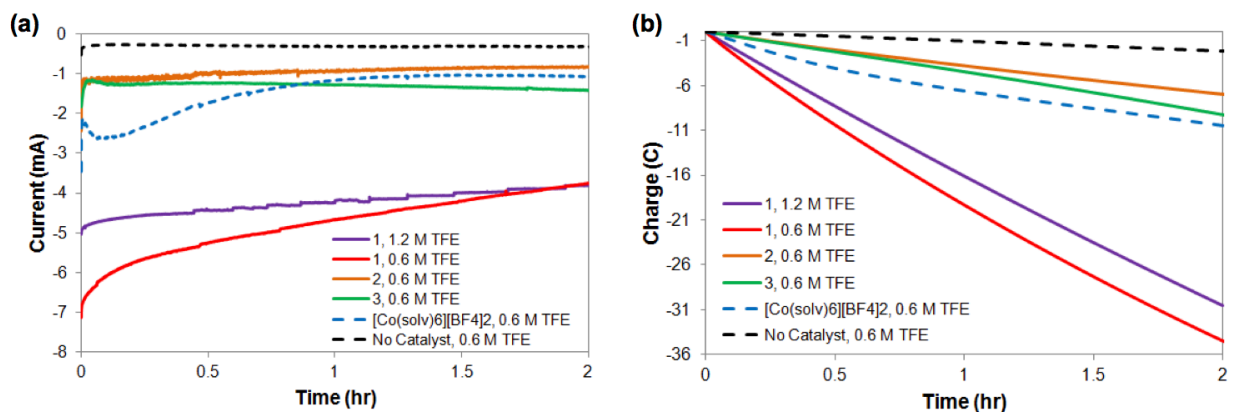


Figure S16. Current (a) and charge (b) traces for controlled potential electrolysis (CPE) experiments over 2 hours for **1** (red and purple), **2** (orange), and **3** (green) at -2.8 V vs. $\text{Fc}^{+/0}$. Electrochemical studies are performed in DMF solutions containing 0.1 M $[\text{nBu}_4\text{N}][\text{PF}_6]$ under an atmosphere of CO_2 and in the presence of 2,2,2-trifluoroethanol (dashed black), Co(II) starting material ($[\text{Co}(\text{solv})_6][\text{BF}_4]_2$, solv = H_2O or MeCN) (dashed blue), and catalyst (0.5 mM each).

Catalyst	[TFE] (M)	$\mu\text{mol CO}$	Faradaic Efficiency (%)	Total TON
1	0.6	160(5)	90(5)	6.4(1)
1	1.2	154(5)	98(2)	6.2(1)
2	0.6	8(1)	23(2)	0.3(1)
3	0.6	<1(1)	<1(1)	—
$[\text{Co}(\text{solv})_6][\text{BF}_4]_2$ (solv = H_2O or MeCN)	0.6	3(1)	6(1)	0.1(1)

Table S3. Faradaic efficiencies and μmol of CO produced for **1**, **2** and **3**, and $[\text{Co}(\text{MeCN})_6][\text{BF}_4]_2$ determined from the controlled potential electrolysis (CPE) experiments performed above at -2.8 V vs. $\text{Fc}^{+/0}$ for 2 hours. Total TON is calculated as $\text{mol}_{\text{CO}}/\text{mol}_{\text{catalyst}}$.

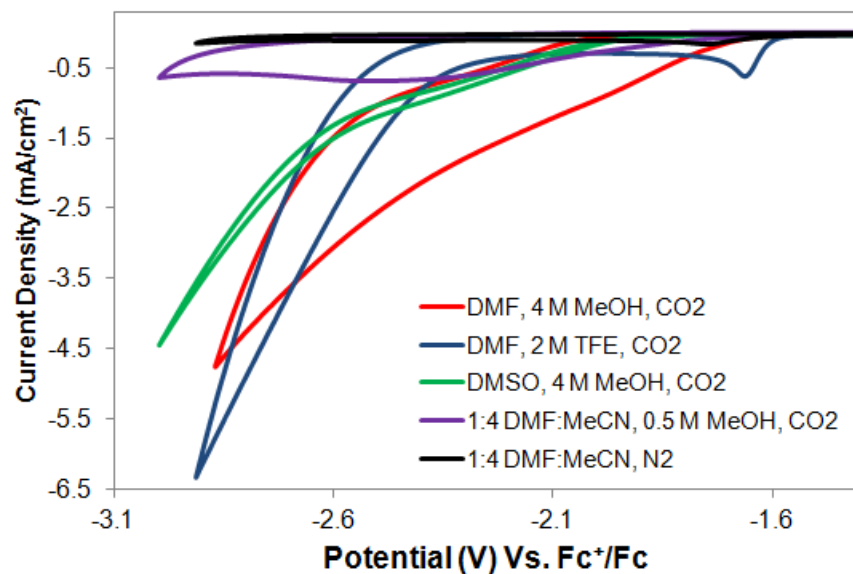


Figure S17. Cyclic voltammograms of $[\text{Co}(\text{H}_2\text{O})_6][\text{BF}_4]_2$ (0.5 mM) under different conditions. 0.1 M $[\text{nBu}_4\text{N}][\text{PF}_6]$. Scan rate is 100 mV/s.

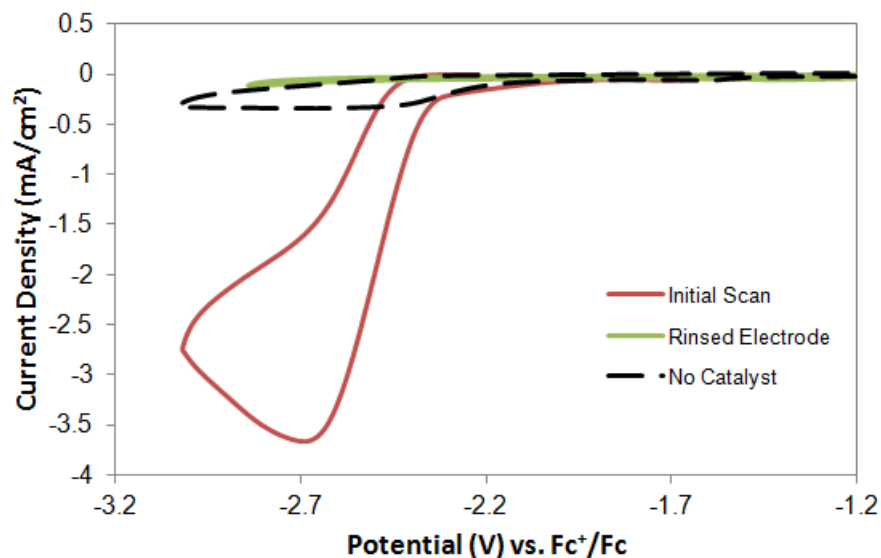


Figure S18. Cyclic voltammograms of **1** (0.5 mM) in a DMF solution containing $[\text{nBu}_4\text{N}][\text{PF}_6]$ (0.1 M), methanol (0.5 M), and CO_2 (1 atm) – red, and of rinsed electrode (3×10 mL DMF) in a fresh DMF solution containing $[\text{nBu}_4\text{N}][\text{PF}_6]$ (0.1 M), methanol (0.5 M), and CO_2 (1 atm) – green. Scan rate is 100 mV/s.

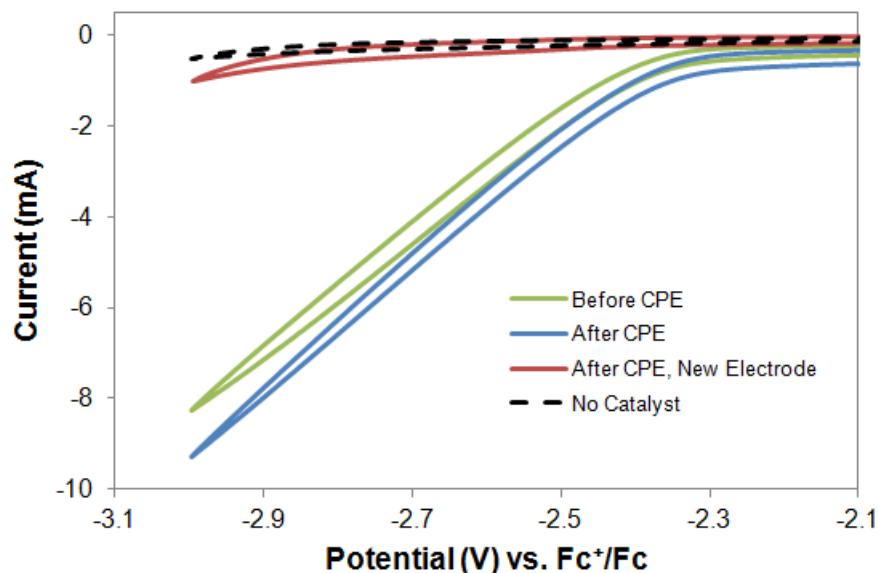


Figure S19. Cyclic voltammograms of **1** (0.5 mM) in a DMF solution containing $[n\text{Bu}_4\text{N}][\text{PF}_6]$ (0.1 M), 2,2,2-trifluoroethanol (0.6 M), and CO_2 (1 atm) before (blue) and after (green) controlled potential electrolysis (CPE). After the controlled potential electrolysis, the working electrode was rinsed (3×10 mL DMF) and its electrochemistry was measured in a fresh DMF solution containing $[n\text{Bu}_4\text{N}][\text{PF}_6]$ (0.1 M), 2,2,2-trifluoroethanol (0.6 M), and CO_2 (1 atm) – red. Scan rate is 100 mV/s.

Catalyst	$E_{1/2}(\text{Co}^{\text{II/I}})$ (V vs $\text{Fc}^{+/0}$)	$E(\text{Co}^{\text{I/0}})$ (V vs $\text{Fc}^{+/0}$)
1	-1.59	-2.36
2	-1.41	-2.58

Table S4. The reduction potentials of complexes **1** and **2**. The electrochemistry of complex **3** is ill defined.

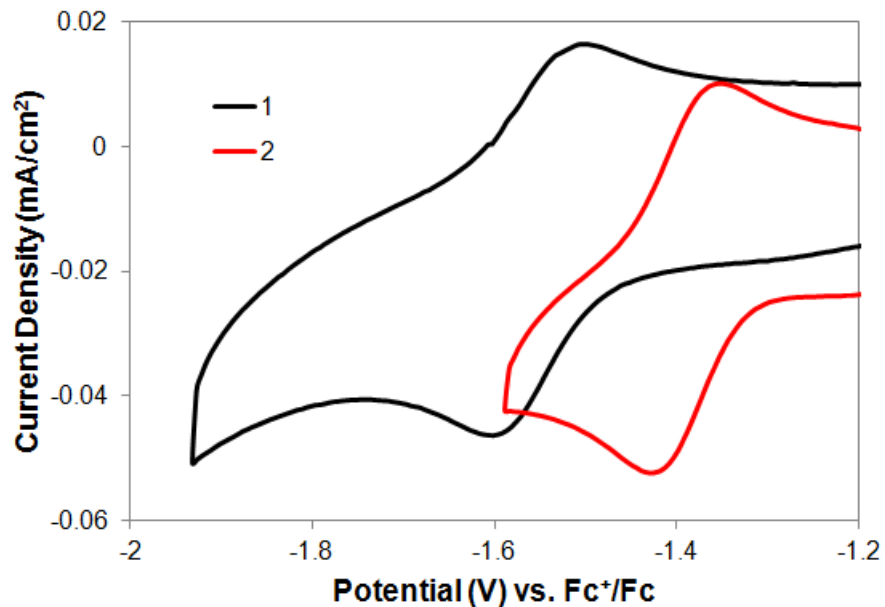


Figure S20. Cyclic voltammograms of 0.5 mM each of **1** (black) and **2** (red) in a DMF solution containing 0.1 M $[n\text{Bu}_4\text{N}][\text{PF}_6]$ under an atmosphere of N_2 displaying the $\text{Co}^{\text{II/I}}$ redox couple. Scan rate is 100 mV/s.

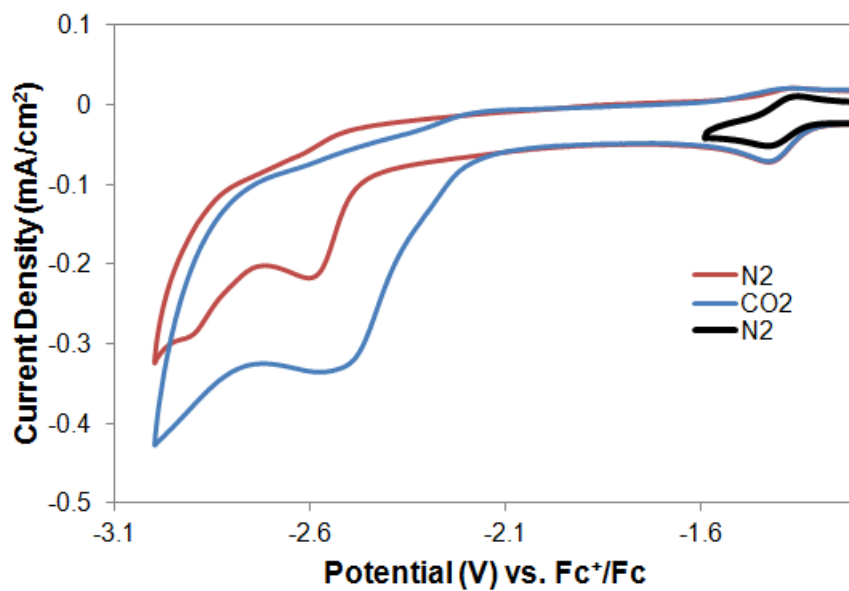


Figure S21. Cyclic voltammogram of 0.5 mM of $[\text{Co}(\text{L}^2)(\text{H}_2\text{O})][\text{BF}_4]_2$ (**2**) in a DMF solution containing 0.1 M $[n\text{Bu}_4\text{N}][\text{PF}_6]$ under an atmosphere of N_2 (black and red) or CO_2 (blue). Scan rate is 100 mV/s.

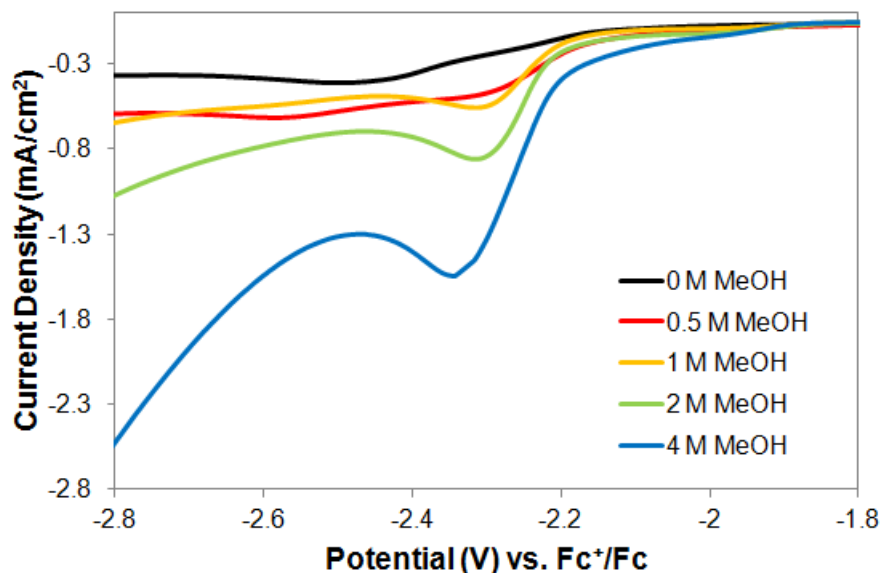


Figure S22. Linear scan voltammograms of **2** (0.5 mM) in a DMF solution containing 0.1 M $[n\text{Bu}_4\text{N}][\text{PF}_6]$ under an atmosphere of CO_2 and in the presence of varying concentrations of methanol. Scan rates are 100 mV/s.

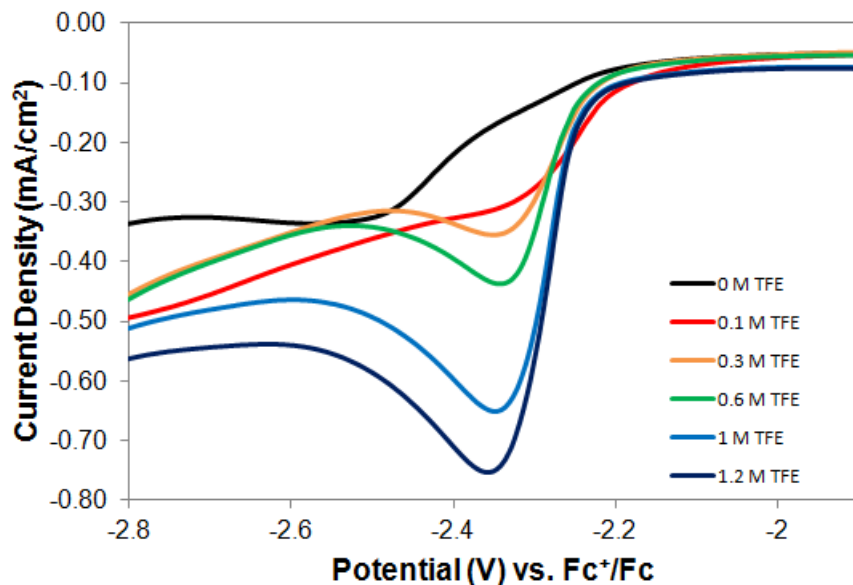


Figure S23. Linear scan voltammograms of **2** (0.5 mM) in a DMF solution containing 0.1 M $[n\text{Bu}_4\text{N}][\text{PF}_6]$ under an atmosphere of CO_2 and in the presence of varying concentrations of 2,2,2-trifluoroethanol. Scan rates are 100 mV/s.

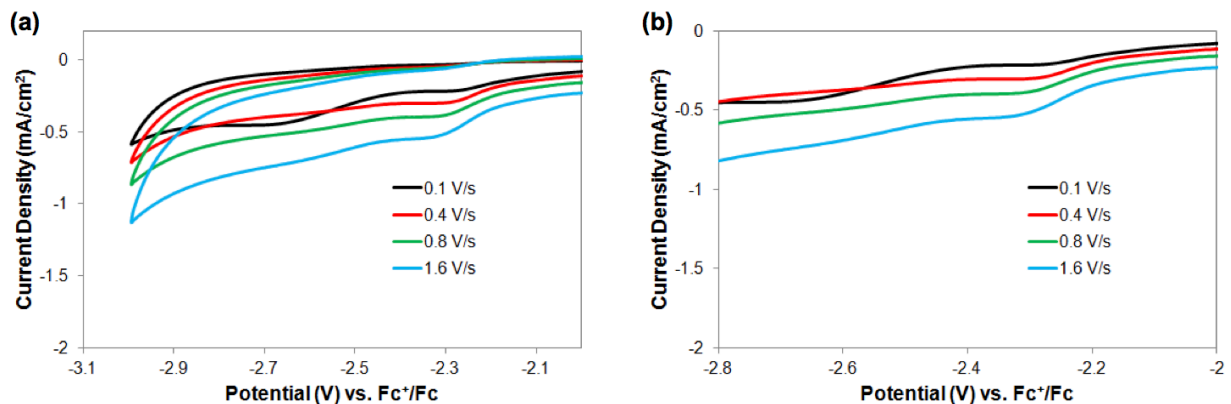


Figure S24. Cyclic voltammogram scan rate dependence of 0.1 mM $[\text{Co}(\text{L}^1)(\text{H}_2\text{O})][\text{BF}_4]_2$ (**1**) in a DMF solution containing 0.1 M $[\text{nBu}_4\text{N}][\text{PF}_6]$ under an atmosphere of CO_2 and in the presence of 2,2,2-trifluoroethanol (0.6 M). Under these conditions catalyst **1** displays catalytic waves as idealized, canonical 'S-shaped', that are scan rate independent. Scan rates vary from 100 to 1600 mV/s.

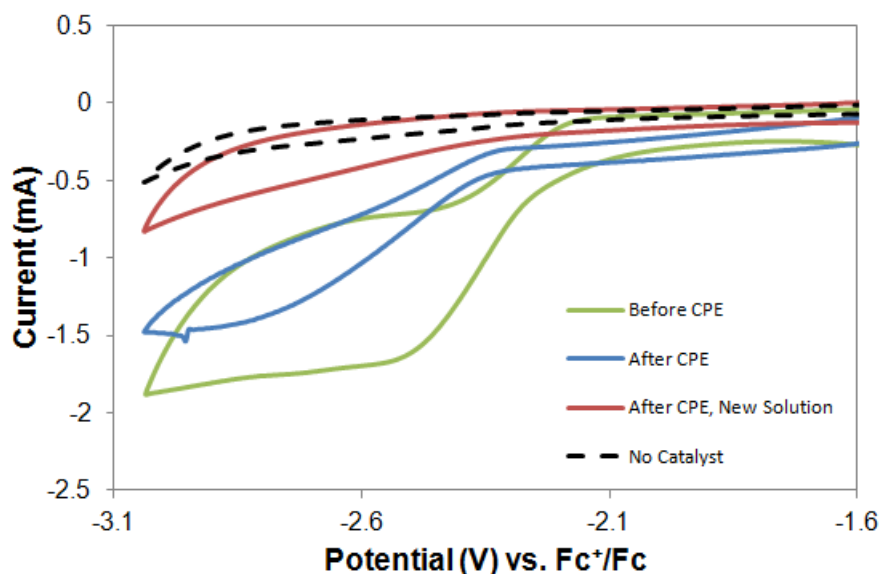


Figure S25. Cyclic voltammograms of **2** (0.5 mM) in a DMF solution containing $[\text{nBu}_4\text{N}][\text{PF}_6]$ (0.1 M), 2,2,2-trifluoroethanol (0.6 M), and CO_2 (1 atm) before (green) and after (blue) controlled potential electrolysis (CPE). After the controlled potential electrolysis, the working electrode was rinsed (3×10 mL DMF) and its electrochemistry was measured in a fresh DMF solution containing $[\text{nBu}_4\text{N}][\text{PF}_6]$ (0.1 M), 2,2,2-trifluoroethanol (0.6 M), and CO_2 (1 atm) – red. Scan rate is 100 mV/s.

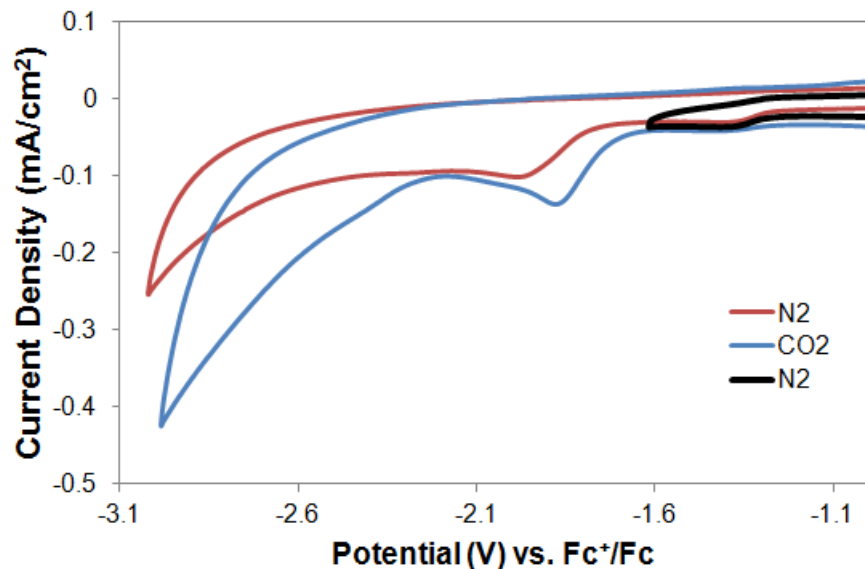


Figure S26. Cyclic voltammogram of 0.5 mM of $[\text{Co}(\text{L}^3)(\text{H}_2\text{O})][\text{BF}_4]_2$ (**3**) in a DMF solution containing 0.1 M $[\text{nBu}_4\text{N}][\text{PF}_6]$ under an atmosphere of N_2 (black and red) or CO_2 (blue). Scan rate is 100 mV/s.

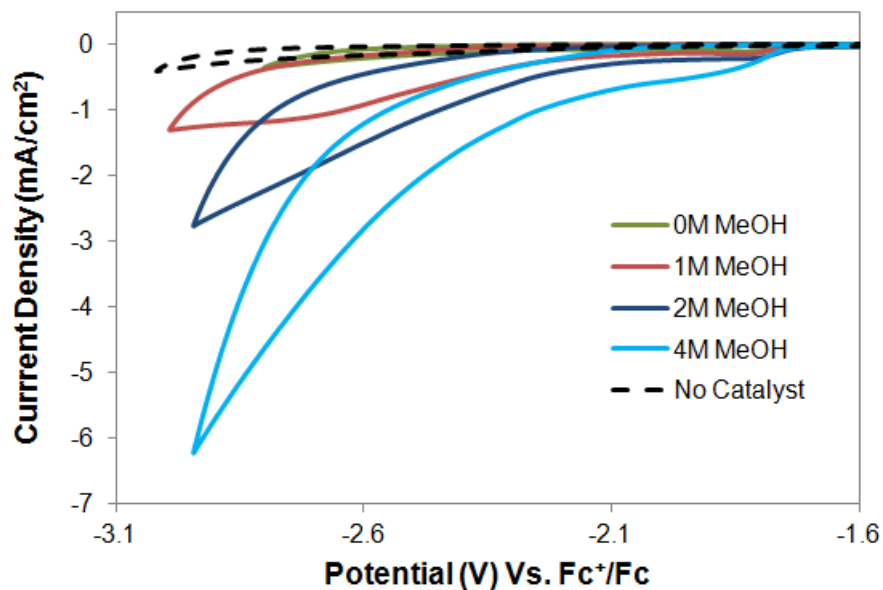


Figure S27. Linear scan voltammograms of **3** (0.5 mM) in a DMF solution containing 0.1 M $[\text{nBu}_4\text{N}][\text{PF}_6]$ under an atmosphere of CO_2 and in the presence of varying concentrations of methanol. Scan rates are 100 mV/s. The change in peak shape is attributed to decomposition.

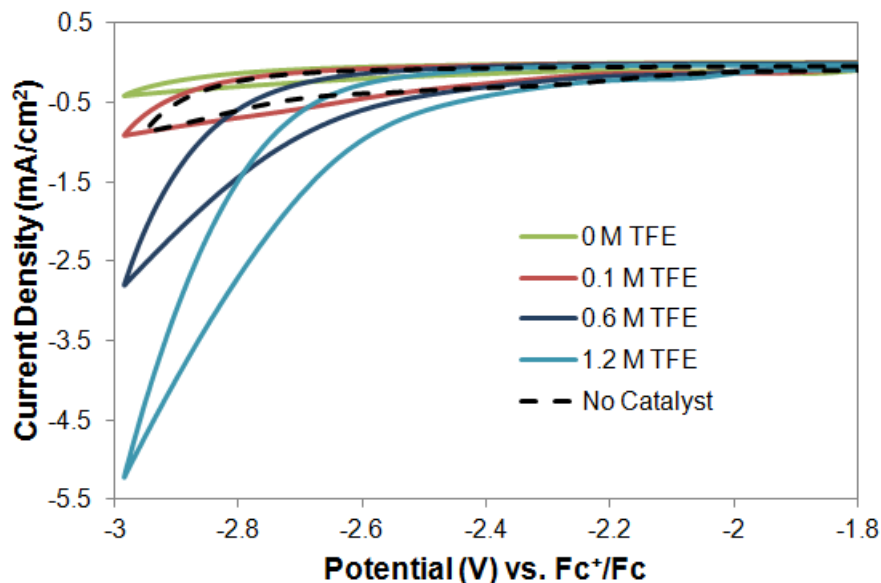


Figure S28. Linear scan voltammograms of **3** (0.5 mM) in a DMF solution containing 0.1 M $[n\text{Bu}_4\text{N}][\text{PF}_6]$ under an atmosphere of CO_2 and in the presence of varying concentrations of 2,2,2-trifluoroethanol. Scan rates are 100 mV/s. The change in peak shape is attributed to decomposition.

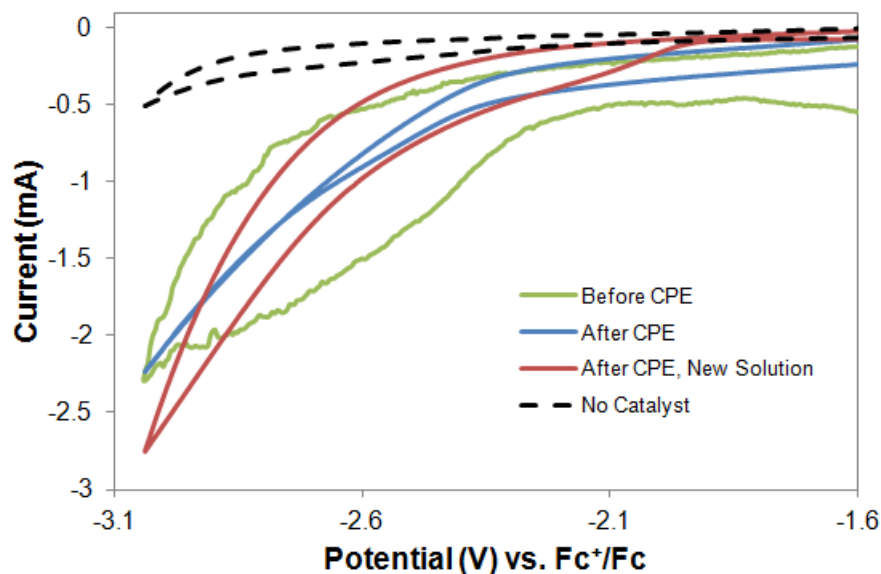


Figure S29. Cyclic voltammograms of **3** (0.5 mM) in a DMF solution containing $[n\text{Bu}_4\text{N}][\text{PF}_6]$ (0.1 M), 2,2,2-trifluoroethanol (0.6 M), and CO_2 (1 atm) before (green) and after (blue) controlled potential electrolysis (CPE). After the controlled potential electrolysis, the working electrode was rinsed (3×10 mL DMF) and its electrochemistry was measured in a fresh DMF solution containing $[n\text{Bu}_4\text{N}][\text{PF}_6]$ (0.1 M), 2,2,2-trifluoroethanol (0.6 M), and CO_2 (1 atm) – red. Scan rate is 100 mV/s.

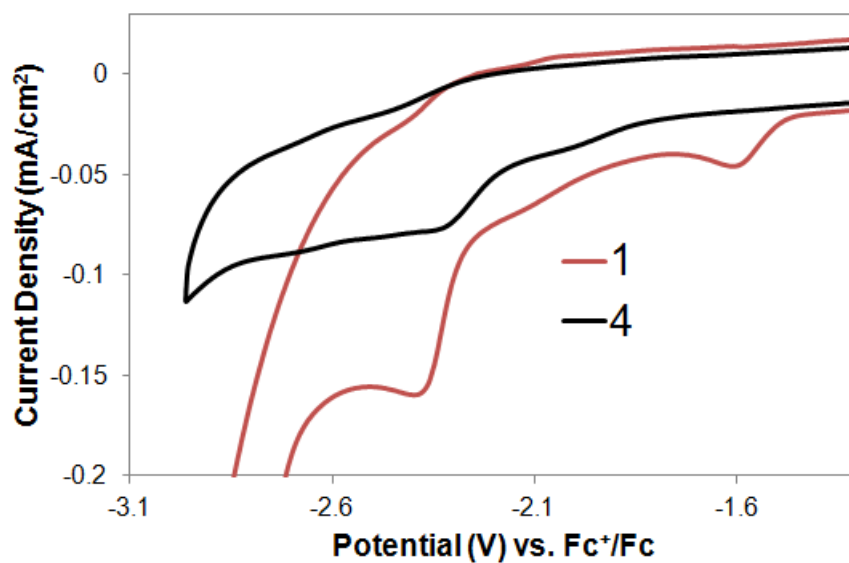


Figure S30. Cyclic voltammograms of 0.5 mM each of **1** (red) and **4** (black) in DMF solutions containing 0.1 M $[n\text{Bu}_4\text{N}][\text{PF}_6]$ under an atmosphere of N_2 displaying the $\text{Co}^{\text{I/0}}$ redox couple. Scan rate is 100 mV/s.

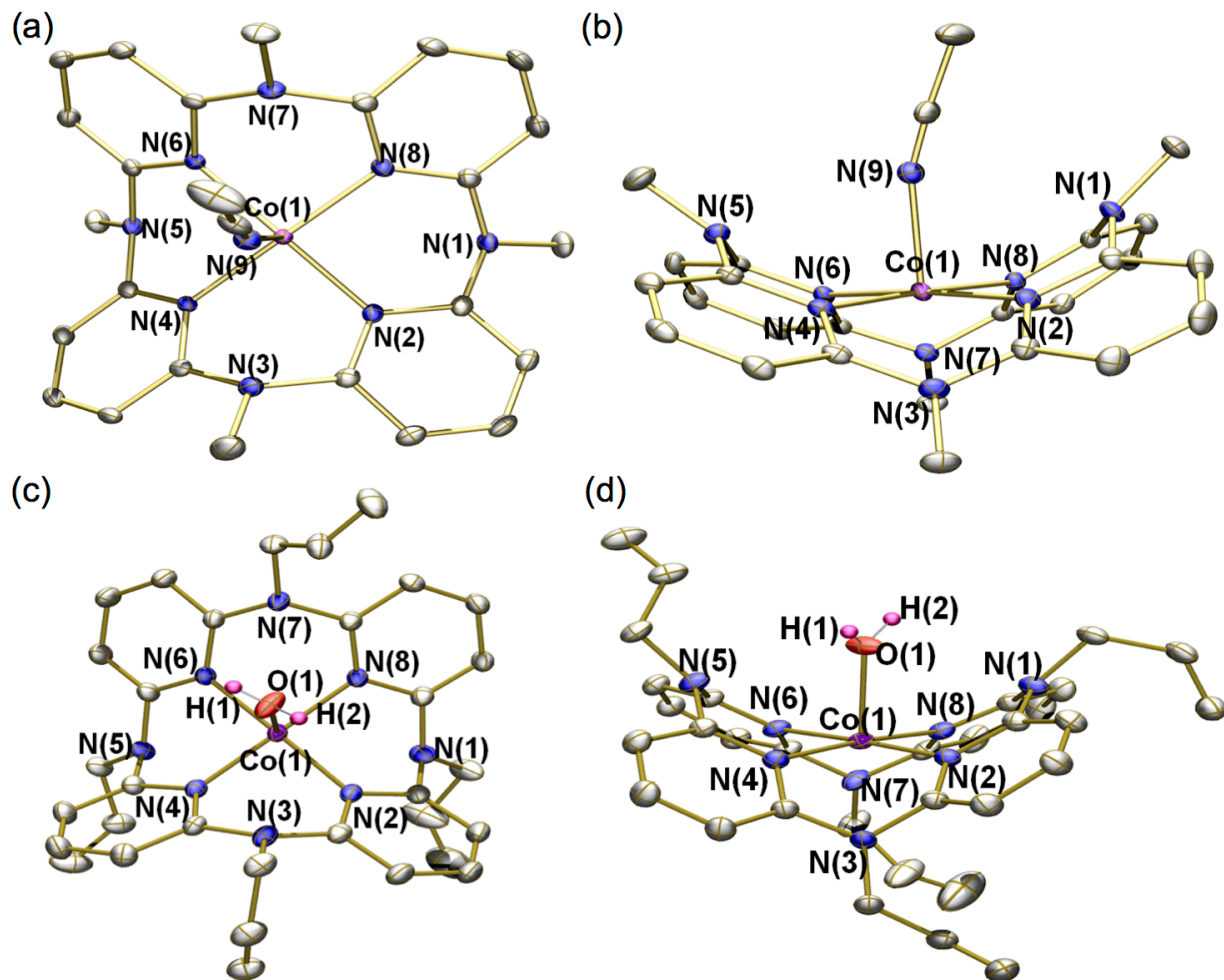


Figure S31. Top and side views of the solid-state structure of **2** (a),(b), and **3** (c),(d). Hydrogen atoms, non-coordinating anions, and solvent molecules are omitted for clarity.

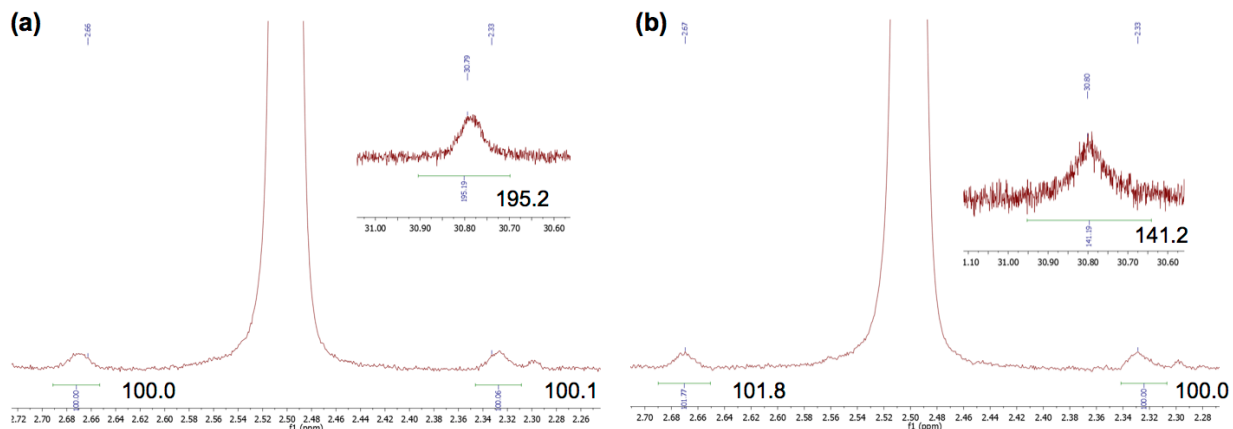


Figure S32. 400 MHz ^1H NMR spectra of a $\text{DMSO-}d_6$ solution containing **1** (0.5 mM), $[\text{nBu}_4\text{N}][\text{PF}_6]$ (0.1 M), 2,2,2-trifluoroethanol (1.2 M), and CO_2 (1 atm) before (a) and after (b) controlled potential electrolysis (CPE) for 2 hours. The peak at δ 30.80 ppm is integrated relative to the solvent ($\text{DMSO-}d_6$) satellite peaks at δ 2.66 and 2.33 ppm. This indicates that 72(5)% of the catalyst **1** remains after the 2 h CPE studies.

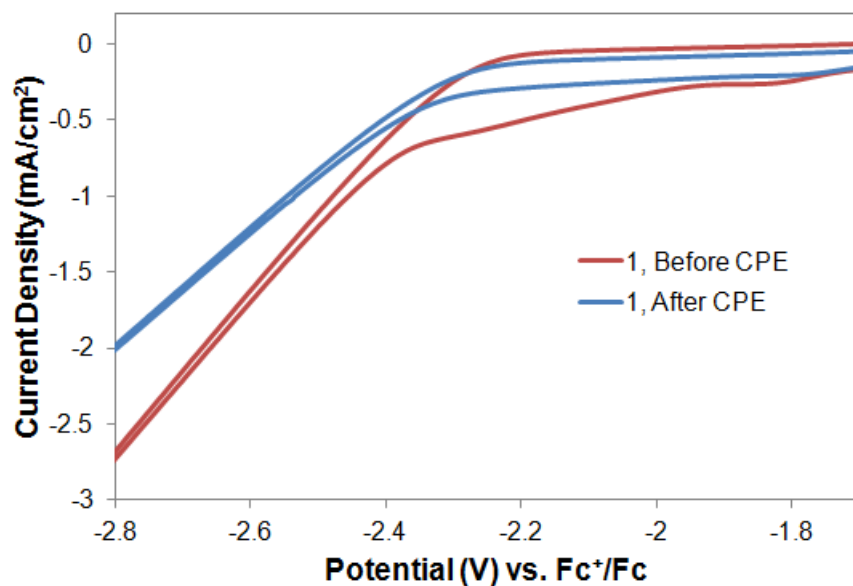


Figure S33. Cyclic voltammograms of **1** (0.5 mM) in a $\text{DMSO-}d_6$ solution containing $[\text{nBu}_4\text{N}][\text{PF}_6]$ (0.1 M), 2,2,2-trifluoroethanol (1.2 M), and CO_2 (1 atm) before (red) and after (blue) controlled potential electrolysis (CPE) for 2 hours. This indicates that 73(5)% of the catalyst **1** remains after the 2 h CPE studies.

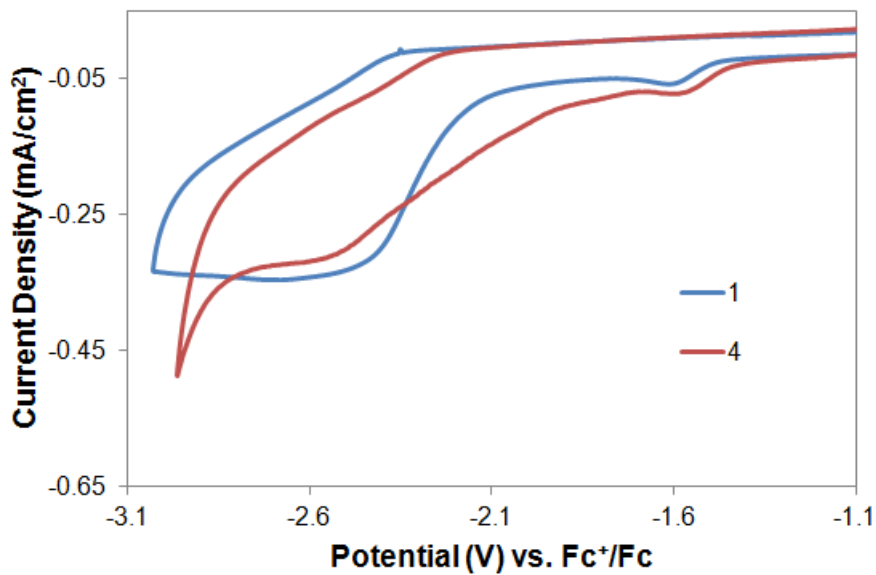


Figure S34. Cyclic voltammograms of 0.5 mM each of **1** (blue) and **4** (red) in DMF solutions containing 0.1 M $[n\text{Bu}_4\text{N}][\text{PF}_6]$ under an atmosphere of CO_2 displaying similar enhanced currents near the $\text{Co}^{\text{I}/0}$ redox couple. Scan rate is 100 mV/s.

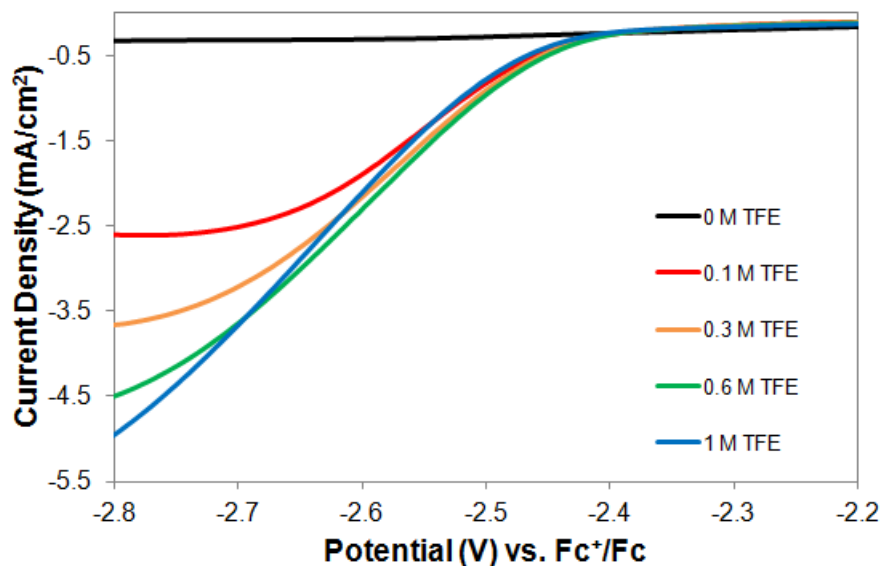


Figure S35. Linear scan voltammograms of **4** (0.5 mM) in a DMF solution containing 0.1 M $[n\text{Bu}_4\text{N}][\text{PF}_6]$ under an atmosphere of CO_2 and in the presence of varying concentrations of 2,2,2-trifluoroethanol. Scan rates are 100 mV/s.

[TFE] (M)	$i_{\text{cat}}/i_{\text{p}}$
0.1	8.6
0.3	12.1
0.6	14.9
1	16.2

Table S5. Table of the peak $i_{\text{cat}}/i_{\text{p}}$ values measured at -2.75 V (vs. $\text{Fc}^{+/0}$) for 0.5 mM **4** in a DMF solution containing 0.1 M $[\text{nBu}_4\text{N}][\text{PF}_6]$ under an atmosphere of CO_2 and with varying amounts of TFE.

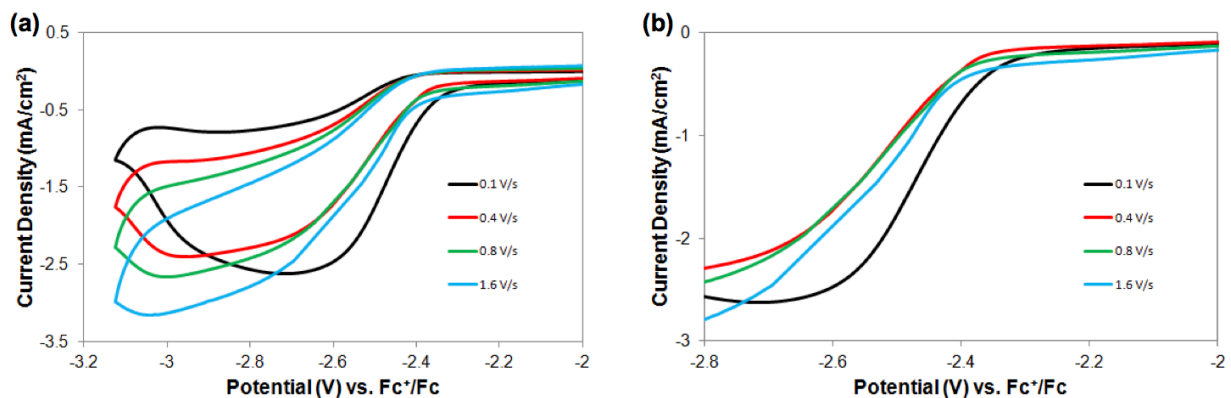


Figure S36. Cyclic voltammogram scan rate dependence of 0.1 mM **4** in a DMF solution containing 0.1 M $[\text{nBu}_4\text{N}][\text{PF}_6]$ under an atmosphere of CO_2 and in the presence of 2,2,2-trifluoroethanol (0.6 M). Under these conditions catalyst **4** displays catalytic waves as idealized, canonical 'S-shaped', that are scan rate independent. Scan rates vary from 100 to 1600 mV/s.

TOF calculations from CVs

Equations 1–3 were used to determine TOF from catalytic CVs. The peak catalytic current (i_{cat}) is given by eq 1. The derivation of eq 1 assumes that pseudo-first-order kinetics apply, i.e., the reaction is first order in catalyst and that the concentrations of the substrates, Q , are large in comparison to the concentration of catalyst. In eq 1, n_{cat} is the number of electrons required for the catalytic reaction ($n_{\text{cat}} = 2$ for the reduction of CO_2 to CO), F is Faraday's constant ($F = 96\,485$ C/mol), A is the surface area of the electrode ($A = 0.07065$ cm² for CVs or 3 cm² for CPE), $[\text{cat}]$ is the catalyst concentration ($[\text{cat}] = 0.5$ mM = 5×10^{-7} mol/cm³), D is the diffusion constant of the catalytically-active species ($\sim 5 \times 10^{-6}$ cm²/s), k_{cat} is the rate constant of the catalytic reaction, and $[Q]$ is the substrate concentration. The concentration of $[\text{CO}_2]$ in DMF is 0.23 M ($= 0.23 \times 10^{-3}$ mol/cm³) as previously reported.²

In eq 2, R is the universal gas constant ($R = 8.31$ J K⁻¹ mol⁻¹), T is temperature ($T = 298.15$ K), n_{p} is the number of electrons in the reversible non-catalytic reaction ($n_{\text{p}} = 1$ for the cobalt aminopyridine system), and v is scan rate ($v = 0.1$ V/s). Dividing eq 1 by eq 2 allows for determination of $i_{\text{cat}}/i_{\text{p}}$ and allows one to further calculate the catalytic rate constant (k_{cat}) and the turnover frequency (TOF), as shown in eq 3. In this equation, the surface area (A) cancels out because the same electrode was used for the experiments under CO_2 and N_2 . D also cancels out because we are assuming that the diffusion constant of the catalytically-active species does not

change significantly under CO₂ or N₂. Using eqs 1–3, we can calculate peak i_{cat}/i_p and TOF values for the cobalt aminopyridine complexes. For these calculations, i_p is determined as the peak current under N₂.

$$i_{cat} = n_{cat} FA[cat]\sqrt{Dk_{cat}[Q]}^{\nu} \quad (1)$$

$$i_p = 0.4463n_p^{3/2}FA[cat]\sqrt{\frac{FvD}{RT}} \quad (2)$$

$$TOF = k_{cat}[Q] = \frac{Fvn_p^3}{RT} \left(\frac{0.4463}{n_{cat}}\right)^2 \left(\frac{i_{cat}}{i_p}\right)^2 \quad (3)$$

By including all the know values and constants in eq (3) we can derive eq (4) for the cobalt aminopyridine complexes.

$$TOF = 1.94 V^{-1} \nu \left(\frac{i_{cat}}{i_p}\right)^2 \quad (4)$$

TOF calculations from CPE

Equations 5–9 were used to determine TOF from CPE data, as previously reported.³ These equations assume that electron transfer to the catalyst is fast, obeying the Nernst law. In eq 5–9, i is the stable current transferred during CPE ($i = \text{charge} \cdot \text{F.E.}/\text{time}$), F is Faraday's constant ($F = 96\,485 \text{ C/mol}$), A is the surface area of the working electrode ($A = 3 \text{ cm}^2$ for CPE), k_{cat} is the overall rate constant of the catalytic reaction, D is the diffusion coefficient ($\sim 5 \times 10^{-6} \text{ cm}^2/\text{s}$), $[cat]$ is the concentration of the catalyst without substrate ($[cat] = 0.5 \text{ mM} = 5 \times 10^{-7} \text{ mol/cm}^3$), R is the universal gas constant ($R = 8.31 \text{ J K}^{-1} \text{ mol}^{-1}$), T is temperature ($T = 298.15 \text{ K}$), $E_{applied}$ is the applied potential during CPE ($-2.8 \text{ V vs. Fc}^{0/+}$), E_{cat}^0 is the standard potential of the catalyst ($-2.36 \text{ V vs. Fc}^{0/+}$), and TOF is the turnover frequency.

$$\frac{i}{FA} = \frac{\sqrt{k_{cat}D[cat]}}{1 + \exp\left[\frac{F}{RT}(E_{applied} - E_{cat}^0)\right]} \quad (5)$$

$$k_{cat} = \frac{i^2 \left(1 + \exp\left[\frac{F}{RT}(E_{applied} - E_{cat}^0)\right]\right)^2}{F^2 A^2 D [cat]^2} \quad (6)$$

$$TOF = \frac{k_{cat}}{1 + \exp\left[\frac{F}{RT}(E_{applied} - E_{cat}^0)\right]} \quad (7)$$

In eq 5–8, $F/RT = 38.92 \text{ V}^{-1}$. Thus, the overall formula for calculating TOF is:

$$TOF = \frac{i^2 \left(1 + \exp\left[\frac{F}{RT}(E_{applied} - E_{cat}^0)\right]\right)}{F^2 A^2 D [cat]^2} \quad (8)$$

When the electrolysis potential is on the plateau of the catalytic wave the following eq can be used to calculate TOF, as previously reported.³

$$TOF = k_{cat} = \frac{i^2}{F^2 A^2 D [cat]^2} \quad (9)$$

Overpotential calculations

Equations 10–11 were used to approximate the overpotential for CO₂ reduction with catalyst **1**. Equation 10, which was previously reported,⁴ was used to determine the thermodynamic potential for CO₂ to CO conversion in the presence of weak Brønsted acids, such as methanol or 2,2,2-trifluoroethanol (TFE). In eq 10, $E_{CO_2/CO(DMF)}^0 = -0.73 \text{ V vs Fc}^{+/0}$,⁴ $pK_{a(MeOH/DMSO)} = 29.0$,⁵ and $pK_{a(TFE/DMSO)} = 23.5$.⁶ In eq 11, $E_{applied}$ is the applied potential during CPE ($-2.8 \text{ V vs. Fc}^{0/+}$). Thus the overpotentials for CO₂ reduction with catalyst **1** in the presence of MeOH or TFE are 0.35 V and 0.68 V, respectively.

$$E = E_{CO_2/CO(DMF)}^0 - 0.0592 \cdot pK_a \quad (10)$$

$$\eta = E_{applied} - E \quad (11)$$

X-Ray Structure Determination for **1**

Low-temperature diffraction data (ϕ - and ω -scans) were collected on a Bruker AXS D8 VENTURE KAPPA diffractometer coupled to a PHOTON 100 CMOS detector with Mo K_α radiation ($\lambda = 0.71073 \text{ \AA}$) from an $I\mu\text{S}$ micro-source for the structure of compound **1**. The structure was solved by direct methods using SHELXS⁷ and refined against F^2 on all data by full-matrix least squares with SHELXL-2014⁸ using established refinement techniques.⁹ All non-hydrogen atoms were refined anisotropically. All hydrogen atoms were included into the model at geometrically calculated positions and refined using a riding model. The isotropic displacement parameters of all hydrogen atoms were fixed to 1.2 times the U value of the atoms they are linked to (1.5 times for methyl groups).

Compound **1** crystallizes in the tetragonal space group $P4_1/amd$ with an eighth of a molecule in the asymmetric unit. The cobalt molecule is located on multiple symmetry elements, which led to a large amount of disorder in the molecule. Due to this disorder and the low data to parameter ratio, all atoms in the model were refined with the help of similarity restraints on the 1,2- and 1,3-distances and displacement parameters as well as rigid bond restraints for anisotropic displacement parameters. Additionally, the two acetone molecules were restrained to be flat. The perchlorate anion was also located on multiple symmetry elements and was refined with the help of enhanced rigid bond restraints in addition to the restraints previously mentioned. The coordinates for the hydrogen atom bound to N(2) and N(12) were located in the difference Fourier synthesis and refined semi-freely with the help of a restraint on the N–H distance (0.91(4) \AA).

Table S6. Crystal data and structure refinement for **1**.

Identification code	P15225	
Empirical formula	$C_{26}H_{28}Cl_2CoN_8O_{10}$	
Formula weight	742.39	
Temperature	100(2) K	
Wavelength	0.71073 Å	
Crystal system	Tetragonal	
Space group	$I4_1/amd$	
Unit cell dimensions	$a = 11.4612(6)$ Å	$\alpha = 90^\circ$
	$b = 11.4612(6)$ Å	$\beta = 90^\circ$
	$c = 23.7694(16)$ Å	$\gamma = 90^\circ$
Volume	$3122.3(4)$ Å ³	
Z	4	
Density (calculated)	1.579 g/cm ³	
Absorption coefficient	0.790 mm ⁻¹	
F(000)	1524	
Crystal size	$0.400 \times 0.200 \times 0.150$ mm ³	
Theta range for data collection	3.042 to 33.140°	
Index ranges	$-17 \leq h \leq 17, -16 \leq k \leq 17, -36 \leq l \leq 36$	
Reflections collected	24164	
Independent reflections	1624 [R(int) = 0.0574]	
Completeness to theta = 25.242°	99.9 %	
Absorption correction	Semi-empirical from equivalents	
Max. and min. transmission	0.7471 and 0.6636	
Refinement method	Full-matrix least-squares on F^2	
Data / restraints / parameters	1624 / 426 / 187	
Goodness-of-fit on F^2	1.098	
Final R indices [$I > 2\sigma(I)$]	$R_1 = 0.0555, wR_2 = 0.1471$	
R indices (all data)	$R_1 = 0.0765, wR_2 = 0.1605$	
Extinction coefficient	n/a	
Largest diff. peak and hole	0.730 and -0.535 eÅ ⁻³	

Table S7. Crystal data and structure refinement for **2**.

Identification code	Alon021815	
Chemical formula	C ₂₆ H ₂₈ B ₂ CoF ₈ N ₉	
Formula weight	698.11 g/mol	
Temperature	100(2) K	
Wavelength	0.71073 Å	
Crystal size	0.094 × 0.360 × 0.848 mm	
Crystal habit	clear yellow-orange prism	
Crystal system	triclinic	
Space group	$P\bar{1}$	
Unit cell dimensions	$a = 10.6914(8)$ Å	$\alpha = 94.5640(10)^\circ$
	$b = 11.7049(8)$ Å	$\beta = 93.0710(10)^\circ$
	$c = 11.9324(9)$ Å	$\gamma = 101.7510(10)^\circ$
Volume	1453.58(18) Å ³	
Z	2	
Density (calculated)	1.597 g/cm ³	
Absorption coefficient	0.678 mm ⁻¹	
F(000)	710	
Diffractometer	Bruker APEX DUO	
Radiation source	fine-focus tube, MoK α	
Theta range for data collection	1.72 to 30.59°	
Index ranges	-15 ≤ h ≤ 15, -16 ≤ k ≤ 16, -17 ≤ l ≤ 17	
Reflections collected	36399	
Independent reflections	8794 [R(int) = 0.0320]	
Absorption correction	multi-scan	
Max. and min. transmission	0.9390 and 0.5970	
Structure solution technique	direct methods	
Structure solution program	SHELXTL XT 2013/1 (Bruker AXS, 2014)	
Refinement method	Full-matrix least-squares on F^2	
Refinement program	SHELXTL XL 2014/7 (Bruker AXS, 2014)	
Function minimized	$\Sigma w(F_o^2 - F_c^2)^2$	
Data / restraints / parameters	8794 / 0 / 420	
Goodness-of-fit on F^2	1.027	
Δ/σ_{\max}	0.001	
Final R indices	7407 data; $I > 2\sigma(I)$ $R_1 = 0.0351$, $wR_2 = 0.0844$	
	all data $R_1 = 0.0455$, $wR_2 = 0.0896$	
Weighting scheme	$w = 1/[\sigma^2(F_o^2) + (0.0386P)^2 + 1.1097P]$ where $P = (F_o^2 + 2F_c^2)/3$	
Largest diff. peak and hole	0.690 and -0.569 eÅ ⁻³	
R.M.S. deviation from mean	0.068 eÅ ⁻³	

Table S8. Crystal data and structure refinement for **3**.

Identification code	Alon072314	
Chemical formula	C ₃₂ H ₃₄ B ₂ CoF ₈ N ₈ O	
Formula weight	779.22 g/mol	
Temperature	100(2) K	
Wavelength	0.71073 Å	
Crystal size	0.110 × 0.334 × 0.428 mm	
Crystal habit	clear orange prism	
Crystal system	triclinic	
Space group	$P\bar{1}$	
Unit cell dimensions	$a = 10.6144(11)$ Å	$\alpha = 103.1970(17)^\circ$
	$b = 12.6739(13)$ Å	$\beta = 104.5760(17)^\circ$
	$c = 14.3737(16)$ Å	$\gamma = 107.7120(18)^\circ$
Volume	1682.4(3) Å ³	
Z	2	
Density (calculated)	1.538 g/cm ³	
Absorption coefficient	0.596 mm ⁻¹	
F(000)	798	
Theta range for data collection	1.55 to 30.56°	
Index ranges	-15 ≤ <i>h</i> ≤ 15, -18 ≤ <i>k</i> ≤ 17, -20 ≤ <i>l</i> ≤ 20	
Reflections collected	36166	
Independent reflections	10077 [R(int) = 0.0268]	
Coverage of independent reflections	97.6%	
Absorption correction	multi-scan	
Max. and min. transmission	0.9370 and 0.7840	
Structure solution technique	direct methods	
Structure solution program	SHELXTL XT 2014/3 (Bruker AXS)	
Refinement method	Full-matrix least-squares on F^2	
Refinement program	SHELXL-2014 (Sheldrick, 2014)	
Function minimized	$\Sigma w(F_o^2 - F_c^2)^2$	
Data / restraints / parameters	10077 / 18 / 477	
Goodness-of-fit on F^2	1.020	
Δ/σ_{\max}	0.001	
Final R indices	8481 data; $I > 2\sigma(I)$ $R_1 = 0.0567$, $wR_2 = 0.1515$	
	all data $R_1 = 0.0675$, $wR_2 = 0.1608$	
Weighting scheme	$w = 1/[\sigma^2(F_o^2) + (0.0838P)^2 + 2.7440P]$ where $P = (F_o^2 + 2F_c^2)/3$	
Largest diff. peak and hole	2.116 and -0.879 eÅ ⁻³	
R.M.S. deviation from mean	0.095 eÅ ⁻³	

Table S9. Crystal data and structure refinement for **4**.

Identification code	ACY_3_28_KC8	
Chemical formula	C ₅₀ H ₄₂ B ₂ CoF ₈ N ₁₄	
Formula weight	1075.56 g/mol	
Temperature	100(2) K	
Wavelength	0.71073 Å	
Crystal system	monoclinic	
Space group	C 1 2/c 1	
Unit cell dimensions	$a = 23.207(2)$ Å	$\alpha = 90^\circ$
	$b = 16.5113(14)$ Å	$\beta = 105.2040(10)^\circ$
	$c = 13.7670(12)$ Å	$\gamma = 90^\circ$
Volume	5090.6(8) Å ³	
Z	4	
Density (calculated)	1.403 g/cm ³	
Absorption coefficient	0.418 mm ⁻¹	
F(000)	2212	
Diffractometer	Bruker APEX DUO	
Radiation source	fine-focus tube, MoK α	
Theta range for data collection	1.53 to 30.59°	
Reflections collected	7132	
Coverage of independent reflections	91.1%	
Absorption correction	multi-scan	
Structure solution technique	direct methods	
Structure solution program	SHELXTL XT 2014/4 (Bruker AXS, 2014)	
Refinement method	Full-matrix least-squares on F^2	
Refinement program	SHELXL-2014/7 (Sheldrick, 2014)	
Function minimized	$\Sigma w(F_o^2 - F_c^2)^2$	
Data / restraints / parameters	7132 / 10 / 357	
Goodness-of-fit on F^2	0.980	
Final R indices	3577 data; $I > 2\sigma(I)$	$R_1 = 0.0689$, $wR_2 = 0.1358$
	all data	$R_1 = 0.1642$, $wR_2 = 0.1618$
Weighting scheme	$w = 1/[\sigma^2(F_o^2) + (0.0763P)^2]$ where $P = (F_o^2 + 2F_c^2)/3$	
Largest diff. peak and hole	0.699 and -0.461 eÅ ⁻³	
R.M.S. deviation from mean	0.086 eÅ ⁻³	

References:

(1) (a) Miyazaki, Y.; Kanbara, T.; Yamamoto, T. *Tetrahedron Lett.* **2002**, *43*, 7945; (b) Uchida, N.; Zhi, R.; Kuwabara, J.; Kanbara, T. *Tetrahedron Lett.* **2014**, *55*, 3070; (c) Zhang, E.-X.; Wang, D.-X.; Huang, Z.-T.; Wang, M.-X. *J. Org. Chem.* **2009**, *74*, 8595; (d) Gong, H.-Y.; Zhang, X.-H.; Wang, D.-X.; Ma, H.-W.; Zheng, Q.-Y.; Wang, M.-X. *Chem. Eur. J.* **2006**, *12*, 9262.

- (2) (a) Sampson, M. D.; Nguyen, A. D.; Grice, K. A.; Moore, C. E.; Rheingold, A. L.; Kubiak, C. P. *J. Am. Chem. Soc.* **2014**, *136*, 5460; (b) Sampson, M. D.; Kubiak, C. P. *J. Am. Chem. Soc.* **2016**, *138*, 1386.
- (3) (a) Costentin, C.; Drouet, S.; Robert, M.; Savéant, J.-M. *Science* **2012**, *338*, 90; (b) Costentin, C.; Robert, M.; Savéant, J.-M. *Chem. Soc. Rev.* **2013**, *42*, 2423.
- (4) Pegis, M. L.; Roberts, J. A. S.; Wasylenko, D. J.; Mader, E. A.; Appel, A. M.; Mayer, J. M. *Inorg. Chem.* **2015**, *54*, 11883.
- (5) Olmstead, W. N.; Margolin, Z.; Bordwell, F. G. *J. Org. Chem.* **1980**, *45*, 3295.
- (6) Bordwell, F. G. *Acc. Chem. Res.* **1988**, *21*, 456.
- (7) Sheldrick, G. M. *Acta Cryst.* **1990**, *A46*, 467.
- (8) Sheldrick, G. M. *Acta Cryst.* **2008**, *A64*, 112.
- (9) Müller, P. *Cryst. Rev.* **2009**, *15*, 57.